Issa *et al.*
Journal of Engineering and Applied Science (2024) 71:132
https://doi.org/10.1186/s44147-024-00467-x

Journal of Engineering and Applied Science

RESEARCH Open Access

Flexural strengthening of LWRC beams using RSHCC reinforced with glass fiber textile mesh

Mohamed E. Issa[1], Nasser F. El-Shafey[1], Ahmed T. Baraghith[2] and Ehab N. Balat[1,3*]

*Correspondence:
ehab.balat@deltauniv.edu.eg

[1] Structural Engineering Department, Faculty of Engineering, Cairo University, Cairo, Egypt
[2] Structural Engineering Department, Faculty of Engineering, Tanta University, Tanta, Egypt
[3] Civil Engineering Department, Faculty of Engineering, Delta University for Science and Technology, Gamasa, Egypt

Abstract

This study aims to explore the flexural behavior of crushed clay brick (CCB) lightweight concrete (LWC) beams strengthened with rubberized strain-hardening cementitious composite reinforced with glass fiber textile mesh layers (GFTM-RSHCC) at the tension side. For this purpose, an experimental investigation consisting of seven simply supported beams, including one un-strengthened specimen, was produced and tested using a monotonic 4-point loading scheme. All specimens had a 120 × 250 mm cross-section, a total length of 2400 mm, and a loaded span of 2200 mm. The studied parameters were the number of GFTM inside the RSHCC (1, 2, or 3) and the thickness of GFTM-RSHCC layer (30 or 40 mm). All the following aspects were tracked: crack pattern, ultimate load, mid-span defection, and ductility. The results show that increasing the number of layers of GFTM and the thickness of RSHCC generally leads to an increase in the ultimate loads and ductility, up to 68% and 83%, respectively, compared to the control beam. Finally, a proposed equation considering the contribution of the GFTM-RSHCC layer was developed to predict the flexural capacity of the strengthened beams. The proposed equation showed good agreement with the experimental results.

Keywords: Crushed clay brick, LWRC beams, Strengthening, Flexural, Glass fiber textile mesh, Rubberized strain-hardening cementitious composite, Concrete

Introduction

Over the last few decades, as development and urbanization have expanded in developing countries, there has been a huge growth in demand for concrete, resulting in its widespread use in the construction sector. However, there are a lot of sustainability and environmental problems generated by the exploitation of coarse aggregate for concrete. Furthermore, some countries have a deficit of normal aggregates due to the consumption of countless tons from many different locations [1]. Lightweight concrete (LWC), essentially composed of lightweight aggregate (LWA), recently presented a challenge for regular-weight concrete (NWC). A great way to lower the building's self-weight is by using LWC [2]. To meet the criteria for LWC status, its density has to exceed 1840 kg/m^3 or below. In addition, LWC provides a large variety of structural and architectural alternatives, and its use in the construction industry is rapidly growing. LWC has been more popular for structural applications in recent

years, particularly in multi-story structures and long-span bridges with high dead loads as outlined in ASTM-C330 [3].

Natural, industrial, and recyclable materials are used as lightweight aggregates [4]. In recent years, construction and demolition (C&D) trash, or waste from building and destroying structures, has grown significantly [5]. Construction and demolition (C&D) trash encompasses materials such as concrete, bricks, tiles, pottery, glass, plastic, wood, and other similar substances [6]. Brick manufacturing waste is a worldwide source of coarse crushed brick (CCB), a lightweight aggregate. Recycling waste as a lightweight aggregate may protect the environment. CCB crushing and sorting produce fine (FCBA) and coarse lightweight aggregate (CCBA). PCB powder may be replaced with cement to increase pozzolanic activity and surface area [7]. Several researches used bricks as coarse aggregate [4] and fine aggregate. Fracture toughness, elastic modulus, and tensile strength are all lower in LWC compared to NWC. These differences might impact the serviceability of structural members [8]. The mix's lightweight aggregate type and supply greatly affect LWC performance [9].

Over decades, a significant number of reinforced concrete (RC) buildings have suffered deterioration as a result of design errors, higher live loads, steel bar corrosion, carbonation, construction defects, and chloride attacks. Enhancing the structural integrity of current reinforced concrete (RC) buildings has become an increasingly important objective to achieve modern design standards. The construction industry has faced a significant challenge in recent years: the need to repair and replace deteriorating reinforced concrete (RC) constructions using different types of composite materials. Currently, there are cementitious materials that are developed to solve the constraints of materials used for repairs or retrofitting. These materials are generally referred to as high-performance fiber reinforced cementitious composites (HPFRCCs) [10]. The capacity to display strain-hardening behavior is one of the main benefits that often motivates the use of High-performance fiber-reinforced cementitious composites or HPFRCC. An example of an HPFRCC is a SHCC (standard strain-hardening cementitious composite). SHCC exhibits enhanced ductility, making it a desirable material for applications such as surface repair and strengthening [11].

Incorporating rubber aggregate into SHCC may improve its ductility, energy absorption, and impact resistance because of its low stiffness and great pliability. Research has shown that using rubber in concrete may enhance its durability by making it more resistant to freezing and thawing, abrasion, and cracking [12]. There are typically three different sizes of rubber aggregates: shredded, crumb, and powder. The use of rubber degrades mechanical qualities, according to previous research [13].

By laying a very thin coating of fiber-reinforced concrete, Martinola et al. [14] observed how strengthened beams affected the structure. Tests conducted by them demonstrated that the suggested method improved the load-bearing capability under strengthening and maintenance scenarios. Baraghith et al. created strain-hardening cementitious composites (SHCC) strengthened with glass fiber textile mesh (GFTM) [15] as an innovative alternative to conventional SHCC that improves upon its performance. On top of that, GFTM-SHCC is often thought of as the perfect corrosion preventive.

Research objective

The flexural behavior of crushed clay brick (CCB) lightweight concrete (LWC) beams strengthened with strain-hardening cementitious composite reinforced with glass fiber textile mesh layers (GFTM-RSHCC) at the tension zone. At shear side, strengthened beams were constructed with carbon fiber sheet (CFS) to prevent the likelihood of premature debonding failure and to significantly enhance the utilization of the adopted strength system. This paper presents an investigation of the flexural behavior of lightweight concrete (LWC) reinforced concrete (RC) beams utilizing crushed clay brick (CCB) as an alternative aggregate. CCB, a significant waste material in construction, offers enticing opportunities for sustainable material adoption. Furthermore, this study examines the efficacy of GFTM-RSHCC concerning various crack patterns, ultimate flexure capacity, load–deflection, failure modes, and the enhancement of ductility. The experimental findings demonstrated the successful use of the GFTM-RSHCC strengthening technique, resulting in enhanced ultimate flexural capacity and improved deformation properties of the specimens under investigation. However, it is important to note that the observed behavior was contingent upon the specific test settings employed. The LWC beams reinforced with GFTM-RSHCC exhibit superior flexural capacity and ductility compared to the control specimen.

Methods

The experimental plan included Seven beams that manufactured using CCB material and subjected to testing using a four-point loading configuration. GFTM-RSHCC layers were incorporated within the tension zone, accompanied by carbon fiber sheets (CFS) to mitigate premature debonding and maximize system strength. Key parameters explored included the number of GFTM-SHCC layers (1, 2, and 3) and RSHCC thickness (20, 30, and 40 mm).

Materials

The design blends shown in Table 1 used crushed clay brick (CCB) aggregate as an eco-friendly substitute for manufacturing lightweight concrete units. Our goal was to find material that was both easily accessible and environmentally friendly that could be used

Table 1 Mix properties of LWC and RSHCC materials (kg/m^3)

Material	LWC	RSHCC
Coarse aggregate	520	–-
Fine aggregate	500	–-
Crushed clay powder	165	–-
Cement	460	1243
Silka fume	44	223
Water	260	292
Superplasticizer	9	14.9
Water-to-binder	0.48	0.20
Quartz sand	–-	149
Polypropylene fiber (12 mm)	–-	14.6
Crumb rubber	–-	10.7

as aggregate. To use the CCB shown in Fig. 1 as coarse aggregate (CCBA), they have particle sizes ranging from 5 to 10 mm. Similarly, for it to function as fine aggregate (FCBA), the particle sizes should be between 250 micromillimeters and 5 mm. Lastly, if the CCB is to be used as crushed clay powder (CCP), the particle sizes should be below 250 micromillimeters.. The strengthening material, rubberized strain-hardening cementitious composites (RSHCC), was mixed according to the quantities shown in Table 1. The RSHCC mix included the utilization of low-heat Portland cement, which has a density of 3.14 g/cm^3. The water-to-binder ratio used was 0.20, and 15% of the cement content was replaced with silica fume in the design. Quartz sand with a particle size less than half a millimeter made up the fine aggregate. A mixture of polypropylene (PP) composed of 2.0% was used to create the fiber that was used for GFTM-RSHCC. The length of the PP fibers was 12 mm, and their diameter was 0.012 mm. Crumb rubber (CR) was substituted for 20% of the amount of silica sand (CR/SS = 0.2 by volume).CR has a specific gravity of 0.95.

The experimental program involves using two-dimensional glass fiber strands to create the Sika fiber mesh 1000 as shown in Fig. 2. These fibers have rectangular cross-sectional dimensions, with a width of 0.85 mm and a thickness of 0.12 mm. Each horizontal and vertical orientation of the mesh had a gap of 5 mm between the individual glass fibers that made up the mesh. Per the manufacturer-supplied datasheet, Table 2 shows the mechanical properties of the glass fiber textile mesh GFTM. Furthermore, the shear and flexural reinforcements have been executed using reinforced bars with dimensions of 10 and 12 mm in diameter, respectively. Uniaxial tensile tests on the bars were done according to ASTM standard citation [16] to establish reinforcement stress–strain parameters. The 10 mm and 12 mm bars showed yield strengths of 452 and 431 MPa and ultimate strengths of 619 and 605 MPa.

Figure 3 shows the steps required to make and apply the epoxy glue. The present study employed MasterBrace 1414 epoxy resin, a product of the local BASF Company. It connected the LWC beams and GTM-RSHCC surfaces. The components for the MasterBrace 1414 epoxy were mixed according to the instructions on the manufacturer's data sheet using a slow-speed mixer with the right paddle. Next, a steel trowel was used to spread a layer of RSHCC. Then, the initial layer of GFTM was progressively encased in

(a) CCBA (b) FCBA (c) CBP

Fig. 1 Crushed clay brick: **a** coarse crushed clay brick aggregate, **b** fine crushed clay brick aggregate, and c clay brick powder

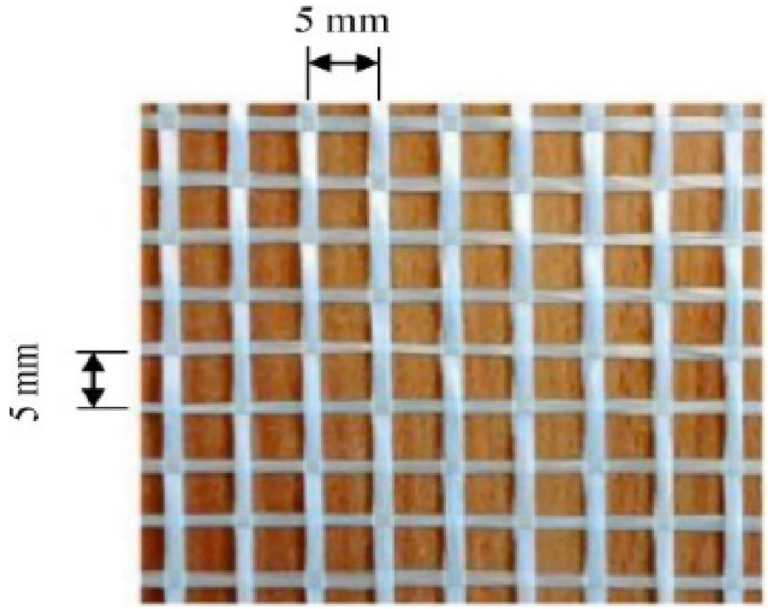

Fig. 2 The used glass fiber textile mesh (GFTM)

Table 2 Geometric and mechanical properties of the used GFTM

One layer nominal thickness (mm)	E_f (GPa)	f_f (MPa)	ε_{uf} (%)
0.12	70	900	1.2

Fig. 3 Applying epoxy resin

the RSHCC. Finally, the GFTM was placed on the specified sides of the LWC beams in the appropriate configurations. If more GFTM layers were needed, identical procedures were followed.

The carbon fiber sheet was shaped to fit the designated area after being cut to size. As shown in Fig. 4, the roller was repeatedly rolled in the direction of the fibers to eliminate bubbles. After the surface has dried, paste the carbon fiber sheet again using the previous steps. Then, evenly distribute the dipping glue over the surface. Prior to conducting

Fig. 4 Carbon fiber sheet (CFS)

Table 3 Mechanical properties of both LWC and RSHCC materials

Mechanical properties	LWC	RSHCC
Dry density Kg/m^3	1830	-
Compressive strength, MPa	32.5	79.8
Splitting tensile strength, MPa	2.67	6.6
Flexural strength, MPa	3.2	8.05
Bonding strength between LWC and RSHCC, MPa	-	2.19

the flexural experiment, the specimens were allowed to naturally dry in the lab for one week after the pasting technique was finished.

LWC and RSHCC Tests

According to ASTM standard [17], three standard cylinders were cast throughout the manufacturing processes of LWC and RSHCC to measure their compressive strengths. There were three cylindrical forms; each has a diameter of 150 mm and a height of 300 mm. The RSHCC materials' tensile stress–strain relationship was determined in the work by Elnagar et al. [18] using the uniaxial tensile testing method. One of the six prisms tested had dimensions of 50-mm thick, 150-mm wide, and 500-mm high. The results are shown in Table 3.

Figure 5 shows the crack mapping that was done for both LWC and RSHCC materials following complete tensile failure to quantify their cracking properties. A finely dispersed pattern of fractures appeared in the RSHCC prism.

Specimens' preparation

Seven lightweight concrete beams were fabricated and subjected to failure testing. Each beam has dimensions of about 120 mm in width and 250 mm in depth, respectively. For internal longitudinal reinforcement, all of the beams that were tested had two 12-mm diameter longitudinal bars stretched across the entire span length on the tension side and two 10-mm diameter longitudinal bars stretched across the entire span length on the compression side. To avoid early shearing of the beams, they have been reinforced by using 10-mm-diameter stirrups placed at intervals of 200 mm. The test for four-point bending test was conducted on all beams with a 2200 mm support-to-support spacing, as seen in Fig. 6.

Fig. 5 Setup and tensile behavior responses of LWC versus RSHCC

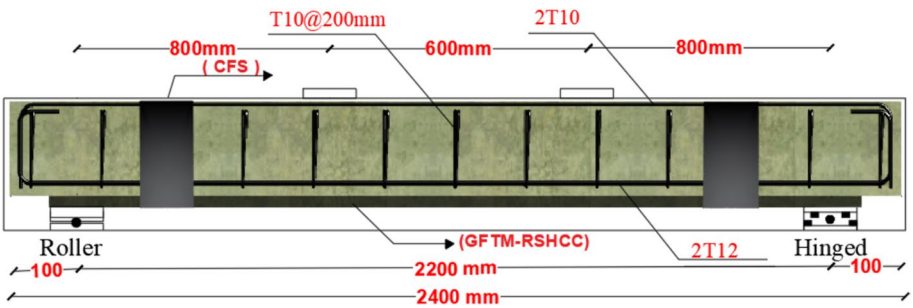

Fig. 6 The concrete dimensions and reinforcement of all specimens

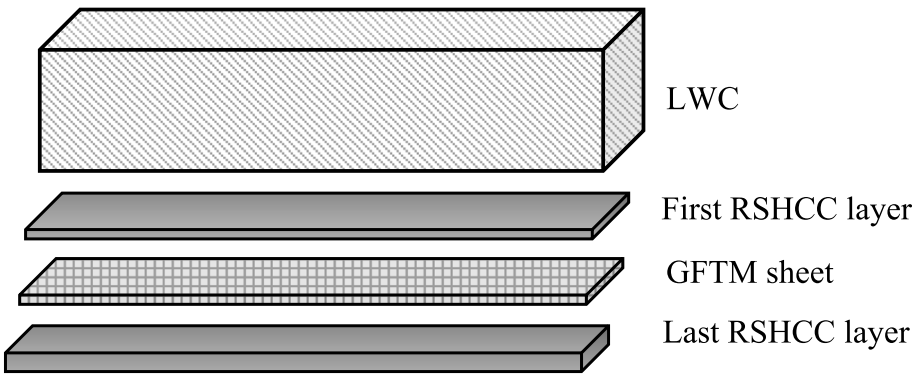

Fig. 7 Strengthening scheme

Installing GFTM-RSHCC laminates

Figure 7 shows a systematic step that was used to construct the strengthening process. To enhance the adhesion between the RSHCC and the bottom surface of the LWC, the tension side surface of each beam was roughened. Preparing the surface primarily aims at "cleaning" the surface by eliminating all potential contaminants, including oil, foreign

particles, dust, laitance, dampness, oxides, and more. The base of the concrete is wetted with water for 24 h before this procedure is applied. For the strengthened specimens: firstly, a layer (5 mm) of RSHCC is applied with a trowel. Secondly, immerse the GFTM sheet in an additional RSHCC layer covered the fiber sheet. The lab photos for the strengthening process are presented in Fig. 8. To prevent debonding of the RSHCC layer, U-wrapping CFRP sheets were applied to the right and left sides of the beam far from two supports at a distance of 100 mm with a width of 50 mm.

Details of specimens

The experimental program included the testing of seven beams. The beams were categorized into two groups, as seen in Table 4.

Test setup

Figure 9 shows the test setup of the monotonic loading tests conducted on all specimens using a four-point loading approach. There was a 600-mm space between the loads, and the beams' effective span was 2200 mm. Utilizing the 900 kN load cell, measure the loads on the beams.

At various loading levels, the vertical deflections were measured using four LVDTs, or linear variable differential transformers. A total of four LVDTs were positioned above the supporting points, two under the span's midpoint and loading point, and one under each of the specimens to calculate their net deflection. Electrical strain gauges, each measuring 6.0 mm in length, were attached to the tensile reinforcement in the mid-span zone to measure the axial strain that was produced by the bars. All experimental measures, such as loads, deflections, and strains, were collected by a data-collecting device while each specimen was being tested.

Results and discussion

Crack pattern and ultimate load

Figure 10 shows the crack pattern of all tested beams. Flexural failure and steel yielding in the mid-spanzone have been observed in the control specimen. At a load of 18.0 kN, cracks developed in the soffit beam section. According to strain data recorded during the test, at a load of 63.0 kN, the beam began to fail when the tension steel yielded, and it finally crushed the concrete on the compression side. During the loading procedure, in the central third of the beam, flexure cracks appeared in the underlying concrete on the tension side. These cracks appeared at loads of 20.0, 21.0, 23.0, and 28.0 kN for the strengthened specimens B2, B3, B4, and B5, respectively. With the growing load, cracks began to form in the strengthening layer and spread upwards into the underlying concrete. The beam sustained the applied load until it failed, with ultimate loads of 70.0, 76.0, 87.0, and 106.0 kN for the strengthened specimens B2, B3, B4, and B5, respectively. According to strain measurements performed during the test, rupture of the strengthening layer occurred at the mid-span, after the yielding of the reinforcing steel bars and before the compression zone concrete crushing.

For the tested group (II), specimens that have been strengthened showed the same failure mechanism as specimens in group (I). Additionally, the flexural cracks appeared at loads of 28.0 and 30.0 kN for the strengthened specimens B6 and B7,

Fig. 8 Strengthening processes in laboratory

respectively. With the growing load, cracks began to form in the strengthening layer and spread upwards into the underlying concrete. The specimen sustained the applied load until it failed, with ultimate loads of 92 and 96.0 kN for the strengthened specimens B6 and B7, respectively. The ultimate, cracking, and yielding loads are shown in

Table 4 Detail parameters of the tested specimens

Group No	Specimen	RSHCC thickness (mm)	No. of GFTM	Objective
Control	B1	---	0	Reference
G1	B2	20	0	No. of GFTM
	B3	20	1	
	B4	20	2	
	B5	20	3	
G2	B6	30	2	Thickness of RSHCC Layer
	B7	40	2	

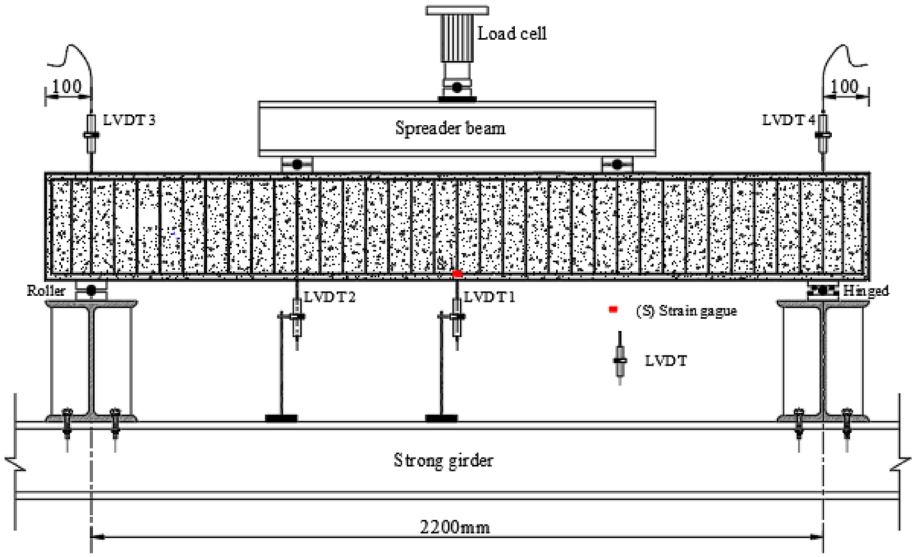

Fig. 9 Test setup and instrumentation

Table 5. The experimental findings, which are presented, demonstrate that the cracking load for each of the strengthened specimens increased to different extents in comparison to the control beam.

Crack width

The maximum width of the crack in the middle third was determined by measuring the crack width with a special microscope. This measurement was done for all beams and plotted against the applied load as shown in Figs. 11 and 12. Regardless of the load, the control beam showed much bigger cracks. When the applied load reached around 18.0 kN, the control beam showed its first cracking. Near the maximum load of 63.0 kN, the crack width reached 0.8 mm on the constant moment region. The beams B2, B3, B4, and B5, which were strengthened with GFTM-RSHCC, had crack widths of 1.1 mm, 0.70 mm, 0.60 mm, and 0.45 mm at the maximum load point, respectively. When compared to the control beam, these numbers show a 78% narrowing of the cracking width. The decrease in width is a result of the strengthening layer's higher layer number which regulates the crack's width. Table 6 summarizes the

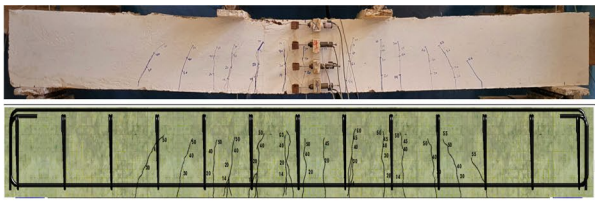

(a) Specimen B1

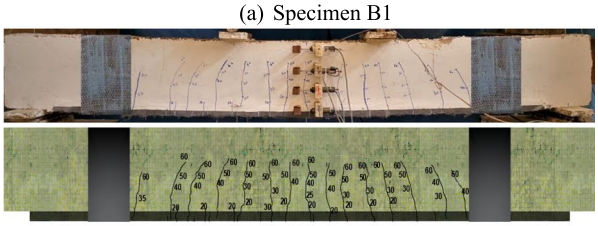

(b) Specimen B2

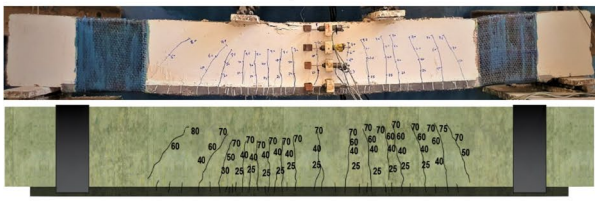

(c) Specimen B3

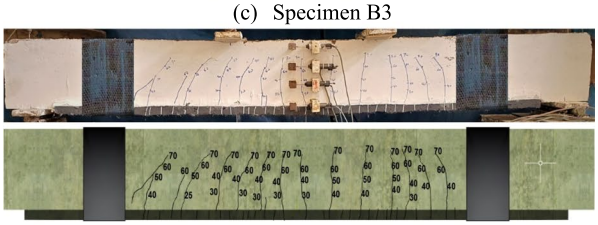

(d) Specimen B4

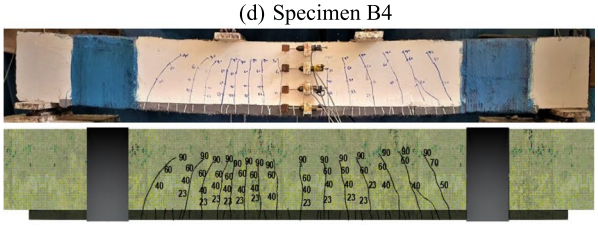

(e) Specimen B5

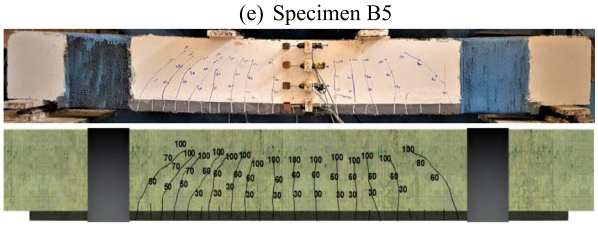

(f) Specimen B6

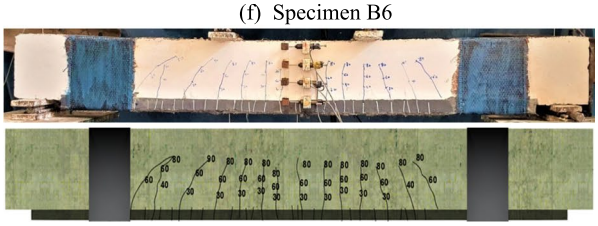

(g) Specimen B7

Fig. 10 Cracks pattern of all tested specimens

Table 5 Cracking and failure loads for each specimen

Group no	Specimen	Load capacity (kN)						Mode of failure
		P_{cr}	Δ_{cr}	P_y	Δ_y	P_u	Δ_u	
Control	B1	18	1.51	54	11.71	63	28.14	Flexural
G1	B2	20	1.26	61	10.75	70	46.78	Flexural
	B3	21	1.53	66	11.03	76	40.51	Flexural
	B4	23	1.41	78	9.78	87	35.9	Flexural
	B5	28	1.83	85	8.51	106	28.55	Flexural
G2	B6	28	1.0	78	8.2	92	33.9	Flexural
	B7	30	0.8	84	10.8	96	27.8	Flexural

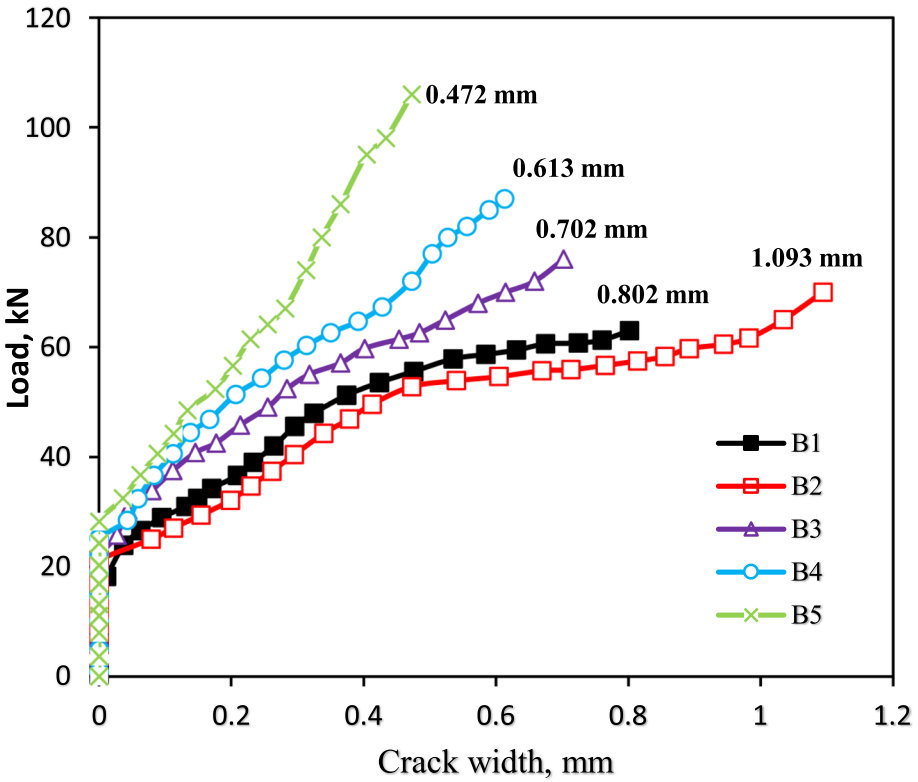

Fig. 11 Load-crack width relationship for group (I)

crack observations made immediately prior to failure for all strengthened specimens, The parameters considered in this study include the average crack spacing (S_{av}), the maximum crack spacing (S_{max}) seen in the strengthening layer, and the number of formed cracks (N) inside the middle third span at failure (P). In an overview of the results, it clearly shows that as the number of glass fiber textile meshes increases, average crack spacing steadily decreases, while the number of produced cracks increases. Beams B2, B3, B4, and B5 developed 27, 38, 35, and 36 cracks, respectively. Increasing the thickness of beams B6 and B7 to 30 and 40 mm allowed them to develop 31 and 37 cracks, respectively. The results presented indicate that a higher

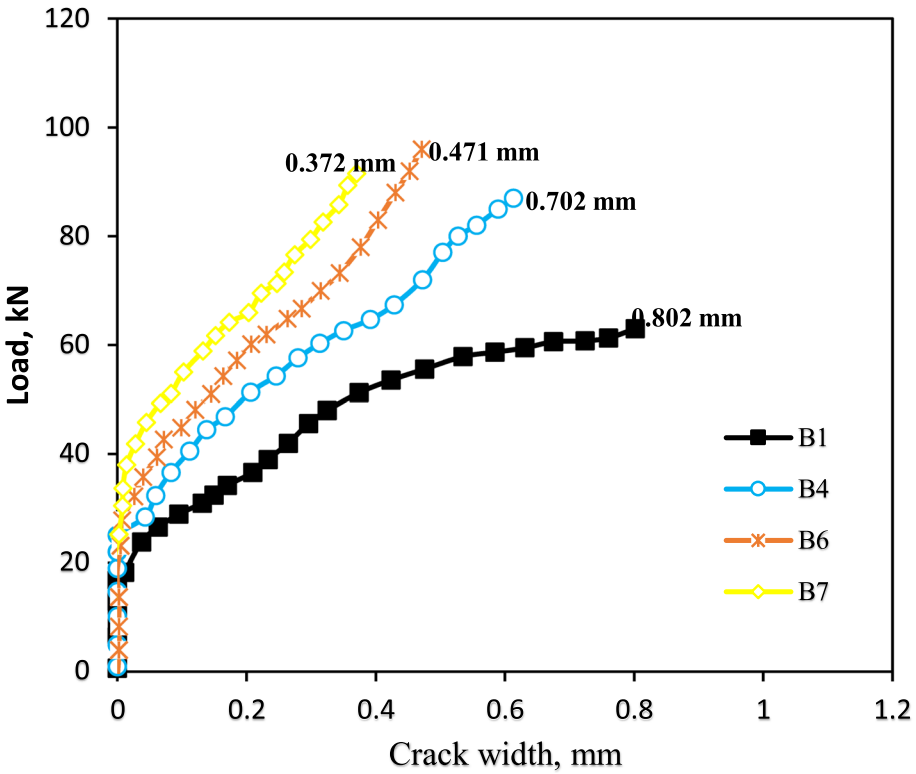

Fig. 12 Load-crack width relationship for group (II)

Table 6 Cracking characteristics of the GFTM-RSHCC layer

Specimen	S_{av} (mm)	S_{max} (mm)
B1	50	115
B2	25	75
B3	20	47
B4	35	44
B5	25	40
B6	50	100
B7	30	40

concentration of GFTM in the strengthening layer improves the flexural behavior by reducing crack width and facilitating more uniform crack distribution.

Load–deflection response

For beams in group (I), the measurement of load–deflection response is shown in Fig. 13. In contrast to the specimens strengthened with GFTM-RSHCC, the control beam (B1) displayed typical elastic and inelastic deflection behavior and ultimately failed as expected because the tensile steel reinforcement yielded before the concrete crushed, resulting in much smaller final deflections. Here are some specific characteristics of each strengthened beam's load–deflection behavior: At first, the beam exhibits

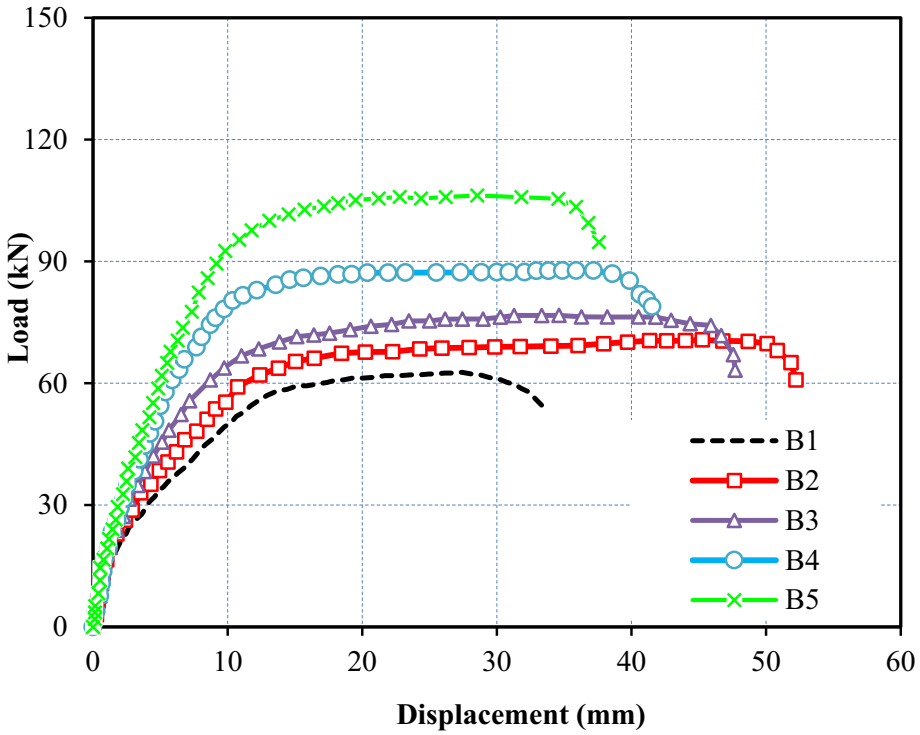

Fig. 13 Load–deflection relationships for group I

linear behavior. However, after it reaches the cracking load, cracks begin to appear in the beam's mid-region. After this point, the curve starts to deviate from its linear trajectory. After the strengthened beam reaches its maximum load, the load gradually decreases until it exceeds the capacity of the control beam (B1). This decrease is caused by a high strain concentration area in the GFTM-RSHCC layer, which leads to a localized failure of the strengthening layer. Following this failure, the GFTM (glass fiber textile mesh) controls the beam's behavior.

Up to the point of maximum load, beams B3, B4, and B5, which were strengthened with 1, 2, and 3 layers, respectively, behaved similarly to the control beam B1 in terms of load deflection. Figure 13 shows that all beams were able to survive inelastic deformation before collapsing after reaching their maximum load, although they did not lose much resistance in the process. Contrary to what was seen with B2, the strengthened beams' load curves softened after reaching their maximum load, and at the peak, the load decreased progressively until it reached a uniform level.

The load–deflection curve of the group II specimens is shown in Fig. 14. The relationship was shown to be linear up to the cracking stage. Failure occurs with loads of 92.0 and 96.0 kN for specimens B6 and B7, respectively, after the cracking stage, when the slope of the curves (secant stiffness) declines with increasing load.

Stiffness

According to Marzouk and Hussein [19], the stiffness of test specimens can be assessed as follows. Initial stiffness, K_i, is defined as the initial slope of load–deflection curve and ultimate stiffness, and K_u is the slope of load–deflection curve at 90% of peak load.

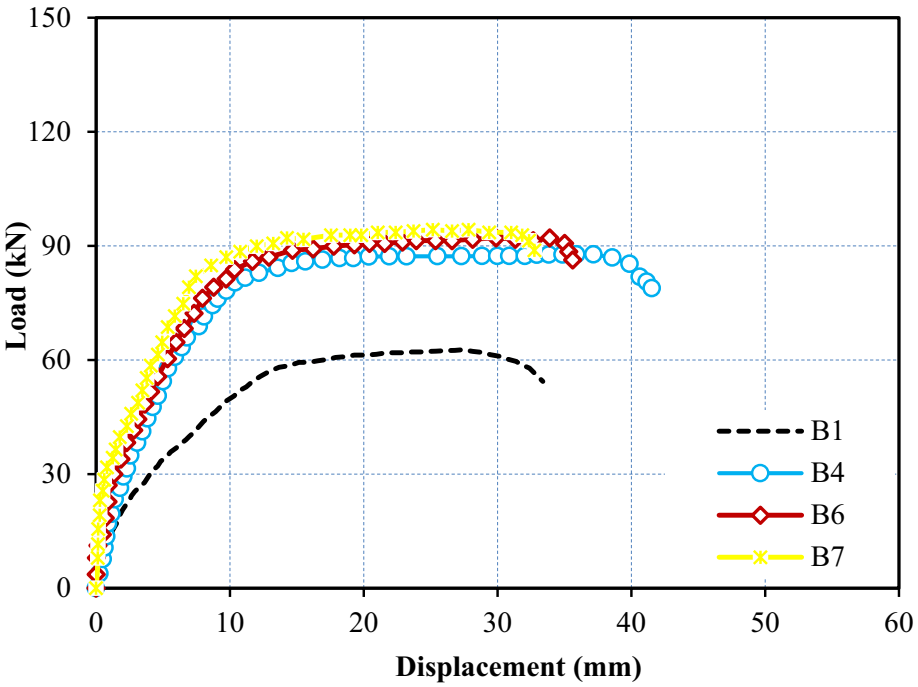

Fig. 14 Load–deflection relationships for group II

Table 7 Stiffness Results for the tested specimens

Group no	Specimens	Stiffness (Kn/mm)	Stiffness (Kn/mm)	Stiffness (Kn/mm)
		K_i	K_u	K_u/K_i
Control	B1	12	11.71	0.97
G1	B2	16	3.53	0.22
	B3	14	4.32	0.31
	B4	16	4.74	0.29
	B5	15	6.57	0.44
G2	B6	28	8.53	0.3
	0.3	0.3	6.94	0.20

Table 7 shows the initial and ultimate stiffness and the stiffness degradation ratio K_u/K_i for the test specimens. The initial and ultimate stiffness increased as the number of GTM.

Ductility analysis

To ensure the secure design and strengthening of any structural part, ductility is a necessary need. Understanding how the new strengthening method known as GFTM-RSHCC affects the ductility of RC components is of the utmost importance. As an indication of ductility for groups I and II, the ductility index (μ_Δ) is defined as the ratio of displacement at the ultimate condition (Δ_u) to curvature at the yield load (Δ_y).

Figures 15 and 16 show that GFTM-RSHCC-strengthened beams have higher displacement ductility indexes (μ_Δ) than the control beam. However, the displacement

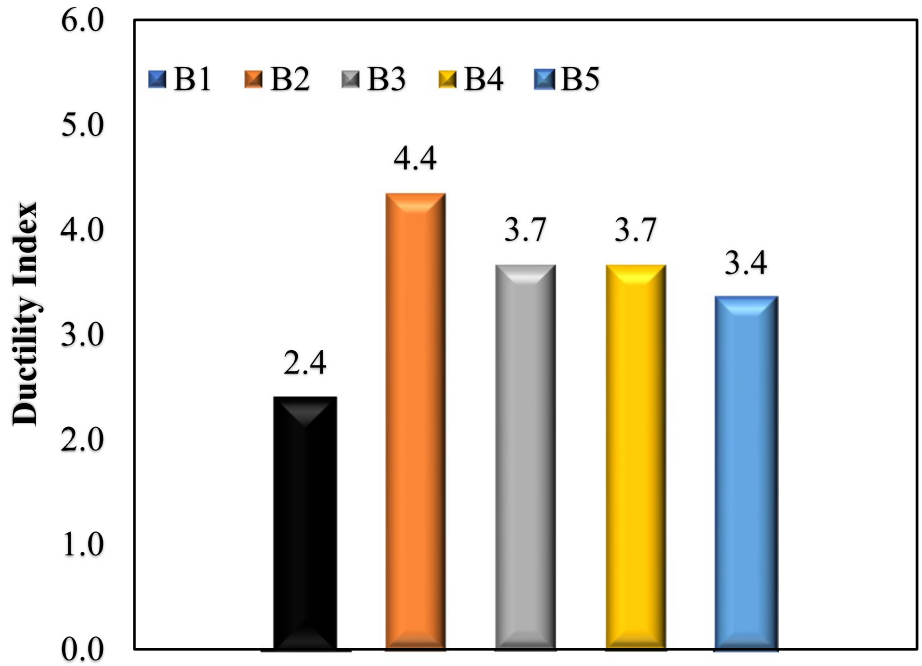

Fig. 15 Ductility index relationships for group I

ductility index (μ_Δ) of strengthened beams (B2 to B7), strengthened with a glass fiber textile mesh (GFTM-RSHCC) layer, is higher than the one obtained for beam B1. The findings seem to imply that using a glass fiber textile mesh layer may effectively improve the ductility of GFTM-RSHCC-strengthened beams. Moreover, one, two, and three layers permitted beams B3, B4, and B5 to obtain displacement ductility index (μ_Δ) of 3.70,

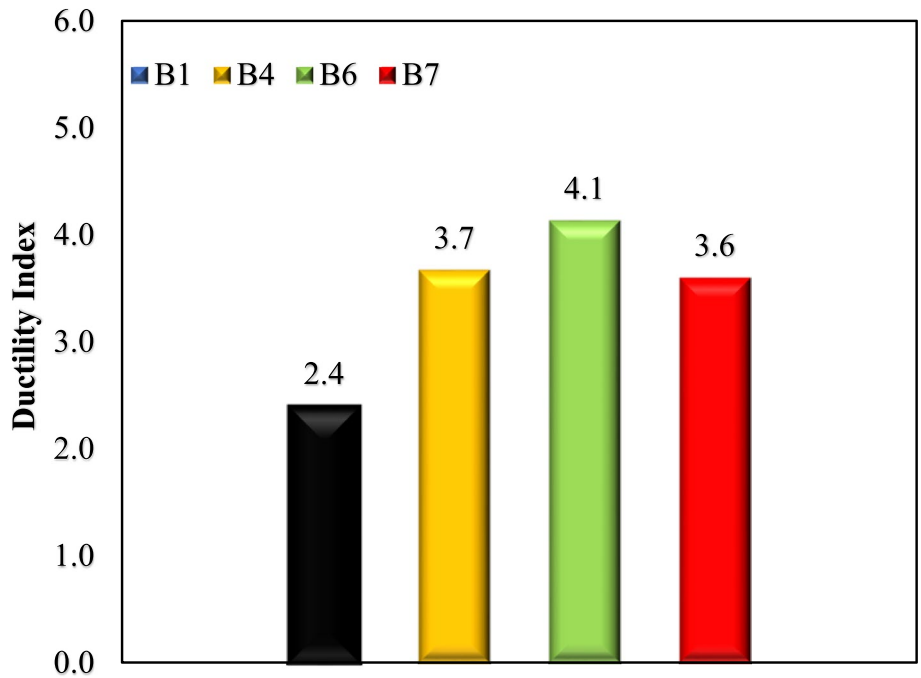

Fig. 16 Ductility index relationships for group II

3.70, and 3.40, respectively, which is suitable to ensure good ductility. Additionally, utilize 30- and 40-mm thickness for strengthened beams B6 and B7 to achieve a displacement ductility index of 4.10 and 2.60, respectively.

Analytical study

Flexural capacity formula using ACI

The American Concrete Institute (ACI 440.2R-02,2005) equation provides a common equation for calculating the theoretical bending strength of simple beams reinforced with external FRP materials, assuming they only have tension steel inside:

$$\mathrm{Mn} = A_s f_s (d_s - \lambda_c/2) + \Psi_f A_f f_{fe} \left(d_f - \lambda_c/2\right)$$

The (ACI 440.2R-02,2005) equations for strengthened beams are adapted to analyze beams with GFTM-RSHCC layers, secondary steel, and embedded reinforcement. This adjustment considers how these elements affect the internal strain and stress patterns within the beam under force and takes into consideration the equilibrium of the section under the forces, as seen in Fig. 17.

The equilibrium equation is as follows:

$$\mathrm{Cc} + \mathrm{Cs}' = \mathrm{T_s} + \mathrm{T_{RSHCC}}$$
$$\mathrm{M_n} = \mathrm{T_s} \times (\mathrm{d_s} - \lambda_c/2) + \mathrm{T_{RSHCC}} \times (\mathrm{d_{RSHCC}} - \lambda_c/2) + \mathrm{C_s} \times (\lambda_c/2\mathrm{d}')$$

Where,

$$\mathrm{C_c} = \gamma \times \mathrm{f_{cu}} \times \mathrm{b} \times \lambda_C$$
$$\mathrm{C_s}' = \mathrm{A_s}' \times \mathrm{f_s}' = \mathrm{A_s}' \times \mathrm{E_s}\ \varepsilon_{cu}\ (\mathrm{c} - \mathrm{d})/\mathrm{c}$$
$$\mathrm{T_s} = \mathrm{A_s} \times \mathrm{f_s} = \mathrm{A_s} \times \mathrm{E_s}\ \varepsilon_{cu}\ (\mathrm{d_s} - \mathrm{c})/\mathrm{c}$$
$$\mathrm{T_{RSHCC}} = \mathrm{A_{RSHCC}} \times \mathrm{f_{RSHCC}} = \mathrm{bt_{RSHCC}} \times \mathrm{E_{RSHCC}} * \varepsilon_{cu} * (\mathrm{d_{RSHCC}} - \mathrm{c})/\mathrm{c}$$

The flow diagram in Fig. 18 summarizes the analytical model's predictions for the flexural nominal moment. Several beams that had been experimentally strengthened and tested up to their failure point were subjected to the proposed equation. For each beam in groups, I and II, Table 8 shows the nominal moment values (M_n, proposed) calculated using the proposed equation in comparison to the experimental capacity values

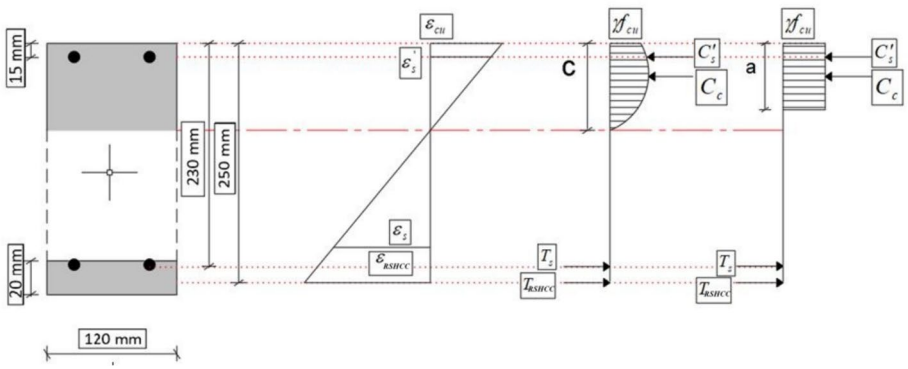

Fig. 17 Stress–strain relationship for RC beams

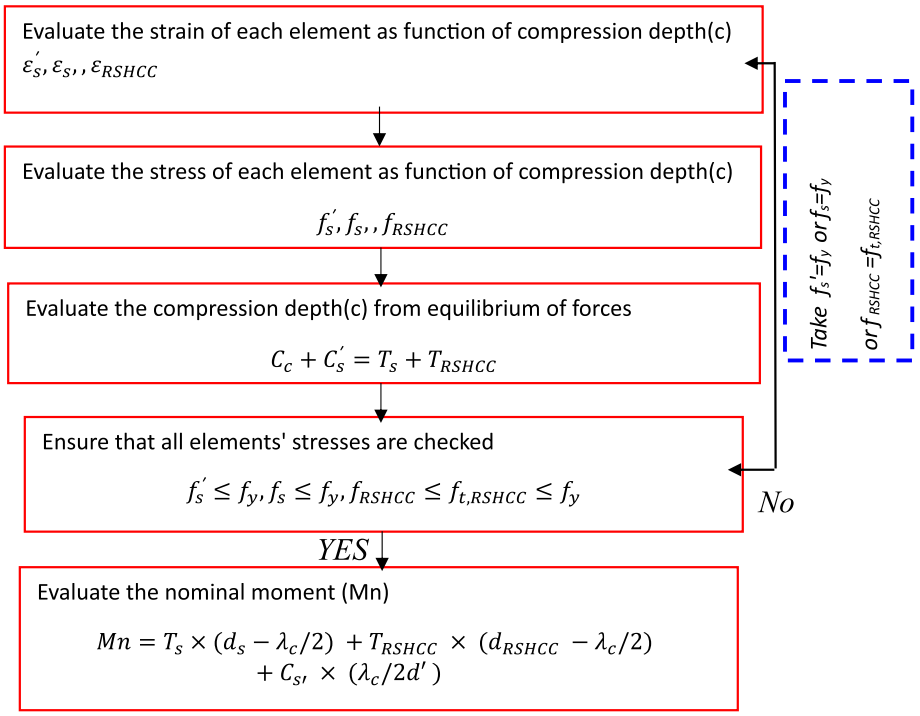

Fig. 18 Nominal moment calculation flow chart

Table 8 Verification of proposed model and experimental results

Specimen	Mn, experimental KN.m	M_n, proposed kN.m	M_n, experimental/ M_n, proposed
B2	28	26.88	1.09
B3	30.4	30	1.07
B4	34.4	33.04	1.08
B5	40	36	1.077
B6	36.8	34.96	1.08
B7	38	36.88	1.12
Average			1.09

(M_n, experimental). This comparison shows that the analytical model that was used was able to accurately predict the nominal capacity, which was close to the results of the experiments.

Conclusions

Based on the abovementioned discussions, the following conclusions can be drawn:

- Compared to the un-strengthened beam (B1), the RSHCC system without GFTM slightly increases cracking (11%), yielding (13%), and ultimate load (11%).
- Compared to the control specimen (B1), strengthened beams showed a significant improvement in both flexural strength and ductility. Strengthened beams

using GFTM-RSHCC showed an increase in ductility of 42% to 83% and a flexural capacity of 11% to 68%.

- Increasing cracking, yielding, and ultimate loads have all been greatly impacted by using the GFTM-RSHCC system from one layer to three layers.
- Compared to the specimen strengthened by a non-layer of GFTM-RSHCC, crack localization in the increasing number of layers of GFTM-SHCC strengthening was delayed. In addition, the number of cracks was dramatically increased.
- Crack width for strengthened beams with GFTM when compared to the control beam, it shows a 78% narrowing of the cracking width.
- The nominal moment for beams strengthened with a GFTM-RSHCC layer was predicted with high accuracy by the used theoretical model.

Abbreviations

LWRC	Reinforced with glass fiber textile mesh
CCB	Crushed clay brick
GFTM-RSHCC	Rubberized strain-hardening cementitious composite reinforced with glass fiber textile mesh
LWA	Lightweight aggregate
NWC	Regular-weight concrete
C&D	Construction and demolition
CCBA	Coarse crushed brick aggregate
FCBA	Fine crushed brick aggregate
CCP	Crushed clay powder
HPFRCC	High-performance fiber reinforced cementitious composites
SHCC	Standard strain-hardening cementitious composite
CFS	Carbon fiber sheets
PP	Polypropylene
CR	Crumb rubber
SS	Silica sand
P_{cr}	Cracking load
P_y	Yielding load
P_u	Ultimate load
S_{av}	Average crack spacing
S_{max}	Maximum crack spacing
N	Number of formed cracks
Δ_{cr}	Cracking deflection
Δ_y	Yielding deflection
Δ_u	Ultimate deflection
M_n	Nominal flexural strength (kN)
A_s	Area of main steel reinforcement (mm^2)
f_s	Stress in tension steel reinforcement (MPa)
d_s	Distance from extreme compression fiber to the neutral axis of steel (mm)
A_f	Area of FRP external reinforcement (mm^2)
f_e	Effective stress in FRP (MPa)
d_f	Distance from extreme compression fiber to the neutral axis of FRP (mm)
k	Ratio of the depth of the equivalent rectangular stress block to the depth of the neutral axis
μ_Δ	Ductility index
ψ_f	Additional FRP strength-reduction factor

Acknowledgements
Not applicable.

Authors' contributions
NF suggested the concept and the methodology of this paper and has the main role in the writing, editing, and revision of the manuscript. EN performed the experimental and analytical methods. AT helped in writing, editing, and revision of the manuscript. I reviewed and edited the manuscript. All authors read and approved the final manuscript.

Funding
This research received no external funding.

Availability of data and materials
Data will be made available on request.

Declarations

Competing interests
The authors declare that they have no known competing financial interests or personal relationships that could have appeared to influence the work reported in this paper.

Received: 27 March 2024 Accepted: 4 June 2024
Published online: 13 June 2024

References

1. Nawaz W, Abdalla JA, Hawileh RA, Alajmani HS, Abuzayed IH, Ataya H, Mohamed HA (2019) Experimental study on the shear strength of reinforced concrete beams cast with Lava lightweight aggregates. Archives of Civil and Mechanical Engineering 19:981–996
2. Yehia S, Abdelfatah A, Mansour D (2020) Effect of aggregate type and specimen configuration on concrete compressive strength. Crystals 10(7):625
3. ASTM A (2017) C330/C330M-17a, Standard specification for lightweight aggregates for structural concrete. ASTM International, West Conshohocken
4. Design of concrete structures (2005) Part 1–2, General rules, structural fire design. Thomas Telford
5. Debieb F, Kenai S (2008) The use of coarse and fine crushed bricks as aggregate in concrete. Constr Build Mater 22(5):886–893
6. Tam VW, Soomro M, Evangelista ACJ (2018) A review of recycled aggregate in concrete applications (2000–2017). Constr Build Mater 172:272–292
7. Wong CL, Mo KH, Yap SP, Alengaram UJ, Ling TC (2018) Potential use of brick waste as alternate concrete-making materials: a review. J Clean Prod 195:226–239
8. Wang Z, Li X, Jiang L, Wang M, Xu Q, Harries K (2020) Long-term performance of lightweight aggregate reinforced concrete beams. Constr Build Mater 264:120231
9. Shin YS, Lee C (2003) Flexural behavior of reinforced concrete beams strengthened with carbon fiber-reinforced polymer laminates at different levels of sustaining load. Structural Journal 100(2):231–239
10. Committee JCI-DFRCC (2003) DFRCC terminology and application concepts. J Adv Concr Technol 1(3):335–340
11. Li VC (2003) On engineered cementitious composites (ECC) a review of the material and its applications. J Adv Concr Technol 1(3):215–230
12. AbdelAleem BH, Ismail MK, Hassan AA (2018) The combined effect of crumb rubber and synthetic fibers on impact resistance of self-consolidating concrete. Constr Build Mater 162:816–829
13. Reda Taha MM, El-Dieb AS, Abd El-Wahab MA, Abdel-Hameed ME (2008) Mechanical, fracture, and microstructural investigations of rubber concrete. J Mater Civ Eng 20(10):640–649
14. Martinola G, Meda A, Plizzari GA, Rinaldi Z (2010) Strengthening and repair of RC beams with fiber reinforced concrete. Cement Concr Compos 32(9):731–739
15. Baraghith AT, Mansour W, Behiry RN, Fayed S (2022) Effectiveness of SHCC strips reinforced with glass fiber textile mesh layers for shear strengthening of RC beams: experimental and numerical assessments. Constr Build Mater 327:127036
16. ASTM A615 (2016) Standard Specification for Deformed and Plain Carbon-Steel Bars for Concrete Reinforcement. ASTM International, West Conshohocken, PA
17. ASTM C39/C39M-21 (2021) Standard test method for compressive strength of cylindrical concrete specimens. ASTM International, West Conshohocken, PA
18. Elnagar AB, Afefy HM, Baraghith AT, Mahmoud MH (2019) Experimental and numerical investigations on the impact resistance of SHCC-strengthened RC slabs subjected to drop weight loading. Constr Build Mater 229:116866
19. Marzouk H, Hussein A (1991) Experimental investigation on the behavior of high-strength concrete slabs. ACI Structural Journal. 88(6):701–713

Publisher's Note